Supplemental Material: A multiscale model of mechanotransduction by the ankyrin chains of the NOMPC channel

David Argudo,[1,*] Sara Capponi,[1,*] Neville P. Bethel,[1] and Michael Grabe[1,†]

[1] *Cardiovascular Research Institute, Department of Pharmaceutical Chemistry, University of California, San Francisco, CA 94143 USA*

(Dated: December 7, 2018)

MATHEMATICS OF IDEAL HELICAL RODS

Modeling Ankyrin chains as idealized helical rods

When a rod lacks excess material twist [1], the spatial configuration is determined fully by the curvature κ and the geometric torsion τ, which are related to the helical angle ζ and the radius R of the helix as (see Ref. [2] for details):

$$\kappa = \frac{\sin\zeta^2}{R}, \qquad \tau = \frac{\sin\zeta\cos\zeta}{R}, \tag{1}$$

where $R > 0$ and $|\zeta|$ range from 0 to $\pi/2$ (for left-handed helices ζ is negative). Please refer to Fig. S1 and Fig. 1 in the main text for a graphical representation.

The end-to-end extension of the helix along its helical axis (the long axis of the spring) is z, and the angle of the end of the helix in the xy-plane (called an end-rotation) is $\Psi = 2\pi N$, where $|N|$ is the number of helical turns. These two quantities are given by:

$$z = l\cos\zeta \quad \text{and} \quad \Psi = l\frac{\sin\zeta}{R}, \tag{2}$$

where l is the helix contour length. Given our mathematical convention, for a left-handed helix, both Ψ and N are negative quantities. Increases in $|N|$ indicate that a deformation causes a helix to overwind (gain more turns), while decreases in $|N|$ correspond to unwinding (lose of turns). Therefore, a left-handed helix overwinds when the end rotations Ψ become more negative, and it unwinds when Ψ becomes less negative (more positive) (see Fig. S1B). The pitch P of a helical configuration can be computed as (again see Ref. [2]):

$$P = \frac{2\pi\tau}{\kappa^2+\tau^2} = 2\pi R\cot\zeta = 2\pi\frac{z}{\Psi}. \tag{3}$$

When $|\zeta| \to \pi/2$ the pitch decreases approaching a tightly coiled spring, whereas when $|\zeta| \to 0$ the pitch increases and the helical rod approaches a straight configuration. The un-deformed initial configuration of the helical rod is defined by the ζ_0 and R_0, which determine the other initial parameters κ_0, τ_0, z_0, Ψ_0, and P_0.

We describe each NOMPC Ankyrin chain as a cylindrical rod with radius $r = 1.0$ nm shaped in the form of a uniform left-handed helix. To extract the parameters characterizing the un-deformed initial configuration, we fit a 4^{th} order curvilinear polynomial to the NOMPC Ankyrin chain extracted from the structure [3] and obtain the values reported in Table S1. The shape corresponding to these values is pictured in Fig. 1B of the main text.

R_0 (nm)	P_0 (nm)	ζ_0 (radians)	z_0 (nm)	l_0 (nm)
3.43	11.73	-1.07	14.0	31.4

Table S1. Geometric parameters describing a single NOMPC Ankyrin chain as an idealized helical rod.

When compression (δz) and end-rotations ($\delta\Psi$) are imposed on the rod, constraints in the pitch and radius of the helix are set. Therefore, for a given initial configuration in the case of infinitesimal displacements δz and rotational motions $\delta\Psi$, from Eq. (2) we obtain:

$$\delta z = -l\sin\zeta_0\delta\zeta, \qquad \delta\Psi = l\frac{\cos\zeta_0}{R_0}\delta\zeta - l\frac{\sin\zeta_0}{R_0^2}\delta R. \tag{4}$$

Equation (4) shows how changes in the helical angle ζ and the radius R affect the chains extension z and rotations Ψ. Alternatively, Eq. (4) can be used to find the changes in ζ and R as a function of the displacements z and rotations Ψ. As described in the main text, Abaqus predicts different behavior between the frictionless model and the rough model. After the NOMPC chains come into contact, in the frictionless model the chains slide past each other leading to an increased radius R, while they further unwind (positive rotations). In the rough model, the chains come into contact in two locations along the curve, and these contact points stick together. This constraint in the rough contact model forces the chains to maintain an approximately constant radius R accompanied by an overwinding effect (negative rotations). This distinct behavior between the two models is explained by the analytic expression in Eq. (4). As a left-handed helix is compressed (negative δz), the first expression in Eq. (4) shows that $\delta\zeta$ is negative (this follows from the mathematical convention that we are using for a left-handed helix where $\zeta_0 < 0$). If the radius is held constant ($\delta R = 0$), then the second expression in Eq. (4) reveals that $\delta\Psi$ must also be negative. Hence, the analytical model predicts that for compression under constant radius R the chains will undergo negative rotations $\delta\Psi < 0$ (overwind), consistent with the rough model observations. On the other hand, Eq. (4) also shows that a chain can only underwind ($\delta\Psi > 0$) if the helical radius expands ($\delta R > 0$), both features that we observe in the Abaqus model for frictionless contact.

Uniform helices in the small deformation regime

In the small displacement limit, the total energy of a helical chain can be approximated by

(see Ref. [2] for details):

$$E_{chain} = \frac{k_{11}}{2}(\Delta z)^2 + k_{12}\Delta z \Delta\Psi + \frac{k_{22}}{2}(\Delta\Psi)^2, \tag{5}$$

where $\Delta z = z - z_0$ is the small compression along the helical axis and $\Delta\Psi = \Psi - \Psi_0$ is the small rotational displacement of the end of the helix. The loads and the displacements are related via the stiffness matrix, which is symmetric and positive definite. The constants k_{11}, k_{12}, and k_{22} that populate the elements of the matrix are determined from the material properties of the rod (the Young's modulus E and the shear modulus G) as follows (see Ref. [2] for details):

$$\begin{bmatrix} F \\ M \end{bmatrix} = \begin{bmatrix} k_{11} & k_{12} \\ k_{12} & k_{22} \end{bmatrix} \begin{bmatrix} \Delta z \\ \Delta\Psi \end{bmatrix} = \begin{bmatrix} \frac{2GI\left(1+\nu\cos^2\zeta_0\right)}{lR_0^2} & \frac{-2GI\nu\sin\zeta_0\cos\zeta_0}{lR_0} \\ \frac{-2GI\nu\sin\zeta_0\cos\zeta_0}{lR_0} & \frac{2GI\left(1+\nu\sin^2\zeta_0\right)}{l} \end{bmatrix} \begin{bmatrix} \Delta z \\ \Delta\Psi \end{bmatrix}, \tag{6}$$

where F is the force acting along the axis of the helix (defined as negative for compression), M is the axial torque, and $\nu = E/2G - 1$ is the Poisson ratio, characterizing the ratio of the axial strain to the transverse strains along a material cross-section [4]. Materials with $\nu > 0$ tend to expand in the direction perpendicular to a compression force and contract in directions transverse to the loading axis when stretched. In our Abaqus models (4 chains), we only apply a compression, Δz, to the system, but due to the the bundle's geometry, the system also undergoes rigid body rotations. In our single chain analysis, the rigid body rotations of the entire bundle can be treated as external applied rotations $\Delta\Psi$ to each individual chain, which give raise to internal moments in the chain. Therefore, Eq. (6) allows us to study analytically the behavior of a single chain, where the effects of the bundle rotations are still considered. In Eq. (6), M represents the external torque that must be applied to keep the chain at a prescribed rotation angle $\Delta\Psi$. This moment M is balanced by an equal, but opposite, internal moment m_z, where m_z is transmitted by a *single* chain to the TRP region. Equation (6) explains why a single NOMPC chain (with $\nu = 0.3$) that overwinds as it compresses exerts a positive moment m_z to the TRP region. First, consider the case of no applied rotation, $\Delta\Psi = 0$, such that there is no winding. According to Eq. (6), under pure compression $M = k_{12}\Delta z$ and Δz is negative. For left-handed helices, ζ_0 varies between 0 and $-\pi/2$; therefore, $\sin\zeta_0 < 0$. Given that the Poisson ratio is positive, k_{12} is positive, the applied torque M is negative, and hence, m_z is positive. Next, add an

overwinding contribution to a left-handed helix, *i.e.* negative applied rotations – $\Delta\Psi$. Then under compression and overwinding, $M = k_{12}\Delta z + k_{22}\Delta\Psi$. The term $k_{22}\Delta\Psi$ is also negative since k_{22} is positive and $\Delta\Psi$ is negative. Hence, for a NOMPC chain under compression that is overwinding, the torque M is negative, which leads to a positive reaction moment m_z. This last result is consistent with our Abaqus observations before the chains come into contact at point # 2 (see Fig. 5D in the main text).

As mentioned earlier, in our Abaqus models we only control the compression parameter Δz, but the entire system undergoes rigid body rotations. In single chain analysis, the end rotations $\Delta\Psi$ are a surrogate variable that allow us to qualitatively explain the behavior of the entire system. For this reason, to get a quantitative estimate of the chain stiffness using the analytical model, we approximate the NOMPC Ankyrin chains as having fixed end rotations ($\Psi = \Psi_0$). In this scenario, Eq. (6) yields a Hookean spring governed by $F = k_{11}\Delta z$. Using the parameters in Table S1 together with the Young's modulus $E = 2.0$ GPa and shear modulus $G = 0.8$ GPa extracted from our MD simulations (see the Results section in the main text) we obtain $k_{11} = 4.0$ pN/nm. Finally, we note that for a tightly coiled helix, we recover the typical spring constant used in previous work (Ref. [5]), where the helical angle ζ_0 approaches $-\pi/2$ yielding $k_{11} = 2GI/(lR_0^2)$ with the contour length $l = 2\pi N R_0$. For the special case of a tightly coiled spring, k_{12} is 0, and consequently, the coupling between rotation and stretch is lost.

Inverting the stiffness matrix gives us the compliance matrix, and allows us to rewrite Eq. 6 to determine the displacements in terms of the loads:

$$\begin{bmatrix} \Delta z \\ \Delta\Psi \end{bmatrix} = \begin{bmatrix} c_{11} & c_{12} \\ c_{12} & c_{22} \end{bmatrix} \begin{bmatrix} F \\ M \end{bmatrix} = \begin{bmatrix} \frac{lR_0^2\left(1+\nu\sin^2\zeta_0\right)}{EI} & \frac{lR_0\nu\sin\zeta_0\cos\zeta_0}{EI} \\ \frac{lR_0\nu\sin\zeta_0\cos\zeta_0}{EI} & \frac{l\left(1+\nu\cos^2\zeta_0\right)}{EI} \end{bmatrix} \begin{bmatrix} F \\ M \end{bmatrix} \tag{7}$$

Equation (7) allows us to study systems where the control parameters are the loads (F and M) instead of the displacements (ΔZ and $\Delta\Psi$). This equation is also useful for studying single molecule experiments where a single chain is subjected to displacements Δz, but is allowed to freely rotate. In that case, the chain is effectively subjected to a zero torque condition, $M = 0$, and the stiffness is given by $F = (c_{11})^{-1}\Delta z$, where $(c_{11})^{-1} \neq k_{11}$.

Uniform helices in the large deformation regime

In the large deformation limit, the strain-energy of a uniform helix is given by the Kirchhoff

theory of inextensible and unshearable rods (see Refs. [2, 6, 7] for details):

$$E_{strain} = \left[\frac{EI}{2}\left(\kappa - \kappa_0\right)^2 + \frac{GJ}{2}\left(\tau - \tau_0\right)^2\right] l, \tag{8}$$

where κ_0 and τ_0 are the curvature and torsion of the un-deformed helix, $J = 2I$ is the polar moment of inertia, and l is the contour length of the center-line of the helical rod which is assumed to be constant, or inextensible. When there is no preferred direction of flexure, the first term penalizes bending deformations, whereas the second term represents the energetic cost of twisting the rod.

When the helical rod is subjected to a vertical force F and torque M along its helical axis, the free energy of the system is:

$$E_{total} = E_{strain} - F\Delta z - M\Delta\Psi, \tag{9}$$

where $\Delta z = z - z_0$ is the compression along the helical axis and $\Delta\Psi = \Psi - \Psi_0$ is the deformation in the end-rotations. Minimization of the total energy (Eq. (9)) with respect to ζ and R yields the following expressions for the force and torque acting on the helix:

$$F = \frac{I}{R^2}\left[\left(E\sin\zeta_0\cos\zeta - 2G\cos\zeta_0\sin\zeta\right)\sin\zeta_0 - \left(E - 2G\right)\sin^2\zeta\cos\zeta\right] \tag{10}$$

and

$$M = \frac{I}{R}\left[E\sin\zeta\left(\sin^2\zeta - \sin^2\zeta_0\right) - G\cos\zeta\left(\sin\zeta\cos\zeta - \sin\zeta_0\cos\zeta_0\right)\right]. \tag{11}$$

Given the initial configuration of the helix, the force (Eq. (10)) and torque (Eq. (11)) are fully determined by the extension z and the rotation Ψ (Eq. (2)). It is important to note that F and M are derived assuming a linear stress-strain relation, *i.e.* small strains, yet these expressions are valid for large deformations, where geometric non-linearities are present.

To obtain the stiffness matrix with the entries defined as a function of the chain's configuration, the infinitesimal axial displacement δz and rotational displacement $\delta\Psi$ need to be considered. The change in the force and moment are:

$$\delta F = K_{11}\delta z + K_{12}\delta\Psi, \qquad \delta M = K_{21}\delta z + K_{22}\delta\Psi, \tag{12}$$

where the axial stiffness is given by

$$K_{11} = \frac{\partial F}{\partial z} = \frac{-1}{l\sin\zeta}\frac{\partial F}{\partial\zeta} = \frac{2GI}{lR^2}\left[\frac{\sin^2\zeta_0}{\sin^2\zeta} + \nu\left(\frac{\sin^2\zeta_0}{\sin^2\zeta} - \sin^2\zeta\right)\right], \tag{13}$$

the rotational stiffness is

$$K_{22} = \frac{\partial M}{\partial \Psi} = \frac{2GI}{l}\left[1 + \nu \sin^2 \zeta\right], \tag{14}$$

and the coupling stiffness is

$$K_{12} = \frac{\partial F}{\partial \Psi} = K_{21} = \frac{\partial M}{\partial z} = \frac{2GI}{lR}\left[(1+\nu)\frac{\sin^2 \zeta_0 \cos \zeta}{\sin \zeta} - \cos \zeta_0 \sin \zeta_0 - 2\nu \sin \zeta \cos \zeta\right]. \tag{15}$$

In the small displacement limit discussed in the previous section, $\zeta \sim \zeta_0$, $R \sim R_0$, and the K_{11}, K_{12}, and K_{22} stiffnesses simplify to k_{11}, k_{12} and k_{22}, respectively.

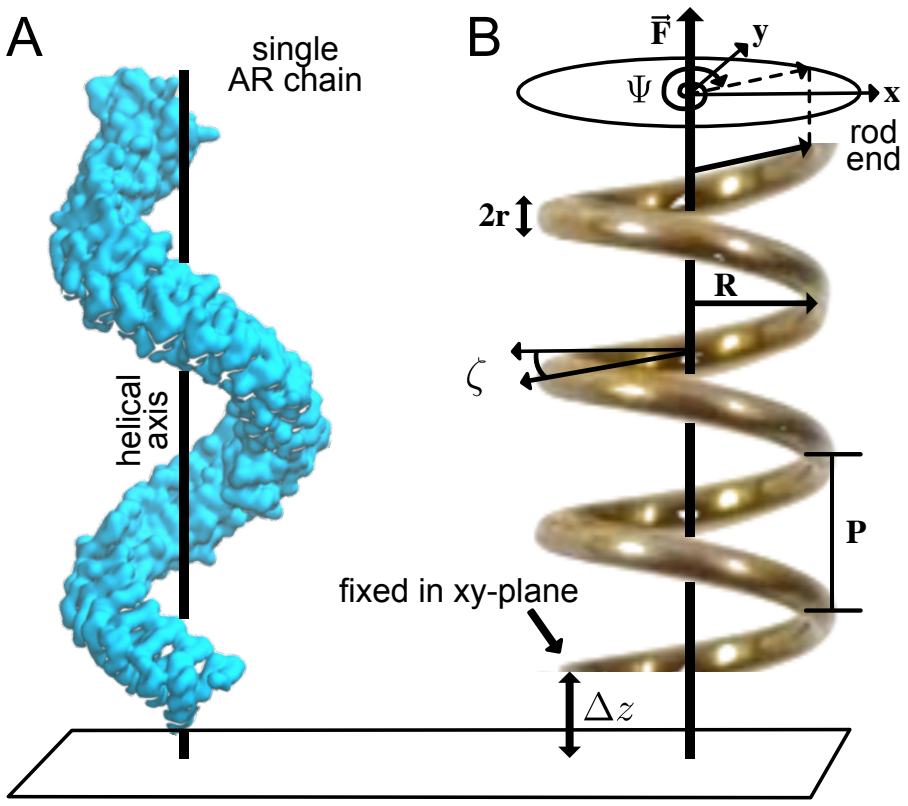

Figure S1. **Helix geometry.** **(A)** Single 29 AR chain from NOMPC indicating the helical axis. This helical rod is left-handed. **(B)** Ideal geometry of a constant pitch, left-handed helical rod used to construct analytical model of NOMPC chain (not to scale with chain in panel A). The rod diameter is $2r$, the helical radius is R, the pitch of the helix is P, the end rotation angle in the xy-plane is Ψ, the helical angle is ζ, and the force on the rod $\vec{F}$ is directed upward along the z-axis. As shown Ψ winds in the xy-plane with negative angular value for a left-handed helix. The end of the rod at the bottom is fixed in the xy-plane, and deflections Δz are upward along the z-axis. The top of the rod is constrained in z, but the end is free to rotate in the xy-plane.

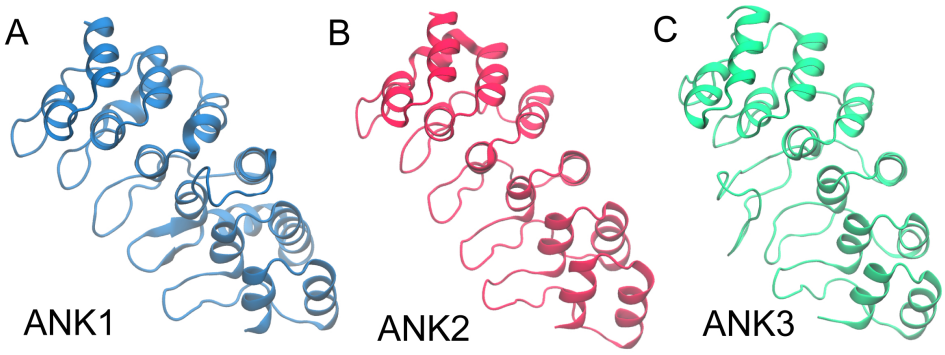

Figure S2. **ANK1, ANK2, and ANK3 structures. (A)** ANK1 (blue) **(B)** ANK2 (red), and **(C)** ANK3 (green) from the NOMPC structure [3] are all presented in new cartoon format. Each segment is composed of 6 AR repeats, yet the composition of the linker regions, the helical twist of the segment, and the conformation of the linkers are all quite different.

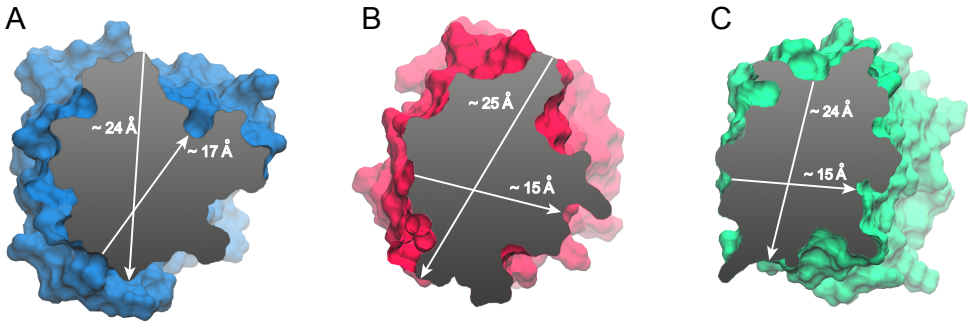

Figure S3. **Cross sectional area of ANK1, ANK2, and ANK3.** The cross sectional area of **(A)** ANK1 (blue), **(B)** ANK2 (red), and **(C)** ANK3 (green) is shown in *gray*. For each panel two distances indicating the heterogenous shape of the area are represented.

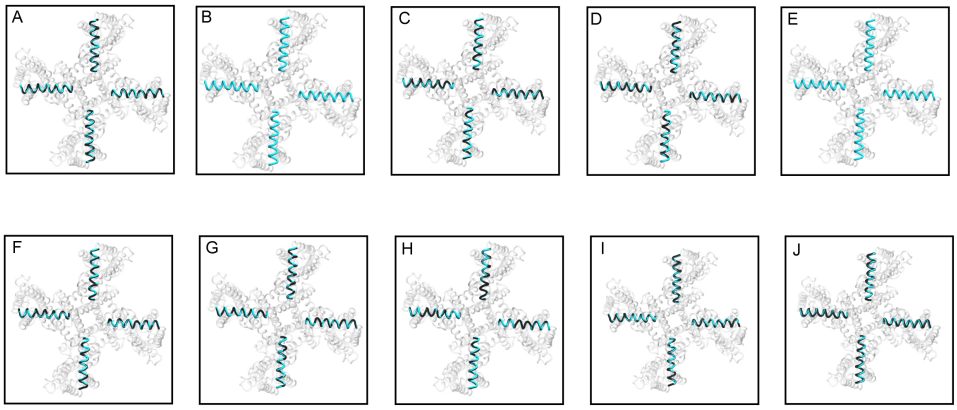

Figure S4. **TRP domain motion in the lowest frequency normal modes of the full, free NOMPC channel.** Cytoplasmic view of the NOMPC channel domain with the TRP domain represented in tube format. Panels **A-J** represent the lowest frequency normal modes 1-10, respectively, of the full free NOMPC channel. To visualize the distortion in the TRP domain corresponding to each mode, we superposed the TRP domains onto each other from the two extreme configurations generated along the normal mode trajectory, and we colored these two configurations black and cyan. All 10 configurations reveal very little to no relative motion in the TRP domain.

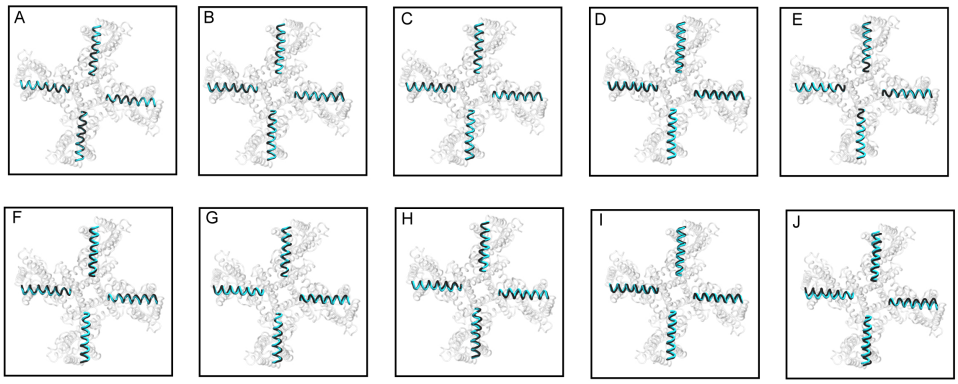

Figure S5. **TRP domain motion in the lowest frequency normal modes of the full, clamped NOMPC channel.** Cytoplasmic view of the NOMPC channel domain with the TRP domain represented in tube format. Panels **A-J** represent the lowest frequency normal modes 1-10, respectively, of the full clamped NOMPC channel. To visualize the distortion in the TRP domain corresponding to each mode, we superposed the TRP domains onto each other from the two extreme configurations generated along the normal mode trajectory, and we colored these two configurations black and cyan. All 10 configurations reveal very little to no relative motion in the TRP domain.

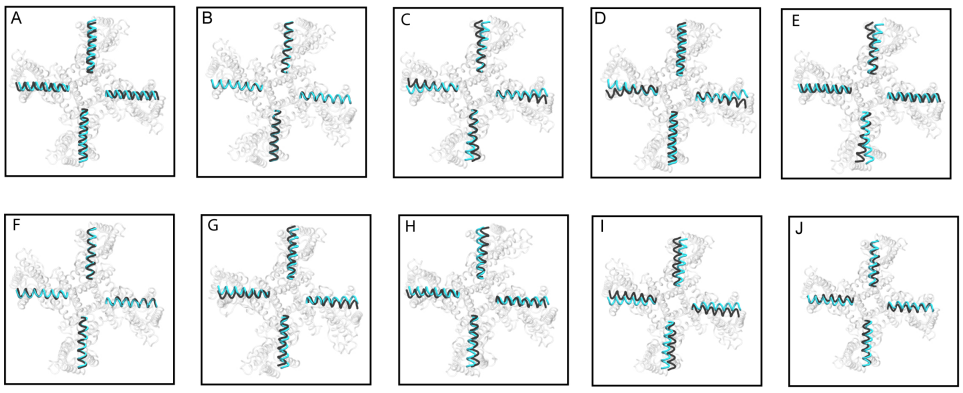

Figure S6. **TRP domain motion in the lowest frequency normal modes of the NOMPC TM domain.** Cytoplasmic view of the NOMPC channel domain with the TRP domain represented in tube format. Panels **A-J** represent the lowest frequency normal modes 1-10, respectively, of the TM domain of NOMPC together with the linker helices and TRP domain. To visualize the distortion in the TRP domain corresponding to each mode, we superposed the TRP domains onto each other from the two extreme configurations generated along the normal mode trajectory, and we colored these two configurations black and cyan. Many of the modes reveal relative changes in the TRP domain during the normal mode motion, but only panel J (mode 10) undergoes a 4-fold symmetric motion consistent with the 4-fold symmetry of the channel.

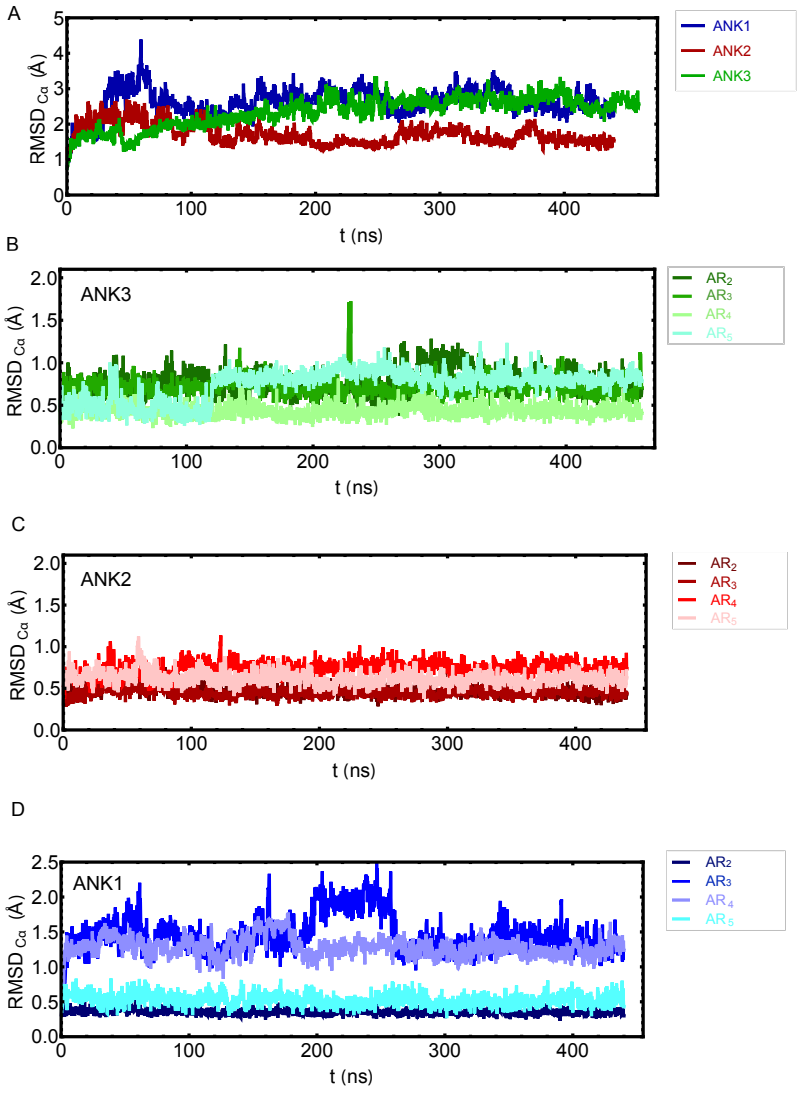

Figure S7. **Stability of ANK1, ANK2, and ANK3 from MD simulations. (A)** The root mean squared displacement (RMSD) of all C_α for ANK1 (*blue*), ANK2 (*red*), and ANK3 (*green*) are plotted as a function of time. **(B-D)** The C_α RMSD of the two, core α-helices from AR_2 through AR_5 are plotted as a function of time for ANK3 (panel B), ANK2 (panel C), and ANK1 (panel D).